Journal of Medicinal Chemistry

Article

pubs.acs.org/jmc

Multistage Screening Reveals Chameleon Ligands of the Human Farnesyl Pyrophosphate Synthase: Implications to Drug Discovery for Neurodegenerative Diseases

Joris W. De Schutter,[†,#] Jaeok Park,[‡,#] Chun Yuen Leung,[†] Patrick Gormley,[§] Yih-Shyan Lin,[†] Zheping Hu,[†,▽] Albert M. Berghuis,[‡,∥,⊥] Judes Poirier,[§] and Youla S. Tsantrizos*[,†,‡,⊥]

[†]Department of Chemistry, McGill University, 801 Sherbrooke Street West, Montreal, Quebec H3A 0B8, Canada

[‡]Department of Biochemistry, McGill University, 3655 Promenade Sir William Osler, Montreal, Quebec H3G 1Y6, Canada

[§]Douglas Mental Health University Institute, 6825 Lasalle, Verdun, Quebec, H4H 1R3, Canada

[∥]Department of Microbiology and Immunology, McGill University, 3775 Rue University, Montreal, Quebec H3A 2B4, Canada

[⊥]Groupe de Recherche Axé sur la Structure des Protéines, McGill University, 3649 Promenade Sir William Osler, Montreal, Quebec H3G 0B1, Canada

Supporting Information

ABSTRACT: Human farnesyl pyrophosphate synthase (hFPPS) is the gate-keeper of mammalian isoprenoids and the key target of bisphosphonate drugs. Bisphosphonates suffer from poor "drug-like" properties and are mainly effective in treating skeletal diseases. Recent investigations have implicated hFPPS in various nonskeletal diseases, including Alzheimer's disease (AD). Analysis of single nucleotide polymorphisms in the hFPPS gene and mRNA levels in autopsy-confirmed AD subjects was undertaken, and a genetic link between hFPPS and phosphorylated tau (P-Tau) levels in the human brain was identified. Elevated P-Tau levels are strongly implicated in AD progression. The development of nonbisphosphonate inhibitors can provide molecular tools for validating hFPPS as a therapeutic target for tauopathy-associated neurodegeneration. A multistage screening protocol led to the identification of a new monophosphonate chemotype that bind in an allosteric pocket of hFPPS. Optimization of these compounds could lead to human therapeutics that block tau metabolism and arrest the progression of neurodegeneration.

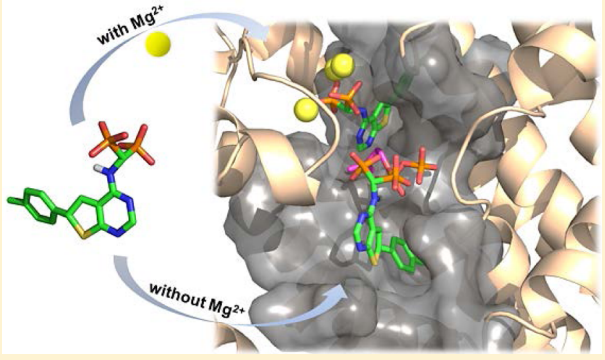

INTRODUCTION

Human farnesyl pyrophosphate synthase (hFPPS) catalyzes the elongation of dimethylallyl pyrophosphate (DMAPP) to geranyl pyrophosphate (GPP) and then to farnesyl pyrophosphate (FPP) via the sequential condensation of DMAPP and then GPP with an isopentenyl pyrophosphate (IPP) unit. The active site cavity of this enzyme is characterized by two highly charged binding subpockets, making the identification of active site inhibitors, with physicochemical properties appropriate for treating nonskeletal diseases, extremely challenging. The allylic subpocket (DMAPP/GPP binding site) is composed of two aspartate-rich motifs that bind the pyrophosphate moiety of the substrate via metal mediated interactions.[1] The other subpocket is lined with basic residues that engage in direct salt-bridge interactions (K57, R60, R113) or water-mediated interactions (R112, R351) with the pyrophosphate moiety of IPP (Figure 1a).[1] The initial occupancy of the allylic subpocket induces a protein conformational change from the "open" to a "partially-closed" state, which fully defines the shape of the IPP binding site. The subsequent binding of IPP leads to the complete closing of the active site cavity, sequestering its substrates from bulk water.[1a,c]

Currently, nitrogen-containing bisphosphonates (*N*-BPs) are the only clinically useful inhibitors of hFPPS; the best examples from this class of drugs include zoledronic acid (**1**) and risedronic acid (**2a**). These drugs bind exclusively to the allylic subpocket and serve as chemically stable pyrophosphate mimics of DMAPP/GPP (Figure 1a).[1] Because of their highly charged nature and affinity for bone, *N*-BPs exhibit poor cell-membrane permeability, rapid clearance from the systemic circulation, and almost negligible distribution to nonskeletal tissues.[2] Consequently, these drugs are mainly used in treating skeletal disorders such as osteoporosis and tumor-induced osteolytic metastases.[3] However, hFPPS is the gatekeeper for the prenylation and activation of many small GTPases that play an essential role in a plethora of cellular functions including cell signaling,[4] proliferation, and synaptic plasticity.[5] Inhibition of

Received: April 22, 2014
Published: June 9, 2014

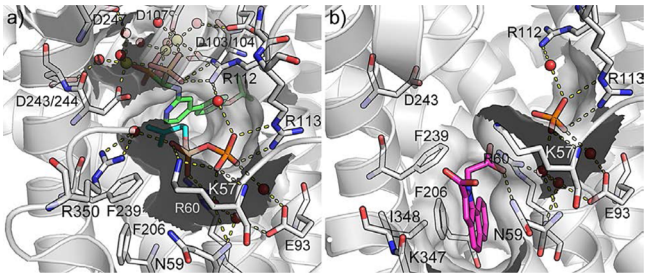

Figure 1. Binding pockets of hFPPS. (a) Structure of the hFPPS/**5m**/IPP complex (PDB ID: 4H5E). (b) Structure of the hFPPS/**4**/Pi complex (PDB ID: 3N6K). The protein surface within 4 Å distance of the bound ligands is rendered semitransparent to indicate the binding pockets. The carbon backbone of IPP, **5m**, and **4** are highlighted in cyan, green, and magenta, respectively. Oxygen, nitrogen, and phosphorus atoms are colored in red, blue, and orange, respectively. Yellow and red spheres represent the Mg^{2+} ions and water molecules, respectively.

hFPPS leads to reduction of cell viability and has been implicated in the antitumor clinical benefits of *N*-BPs.[3,6] Inhibition of hFPPS also induces activation of $\gamma\delta$ T cells, providing immunosurveillance against tumors.[7] Additionally, overexpression of hFPPS and high levels of farnesyl pyrophosphate (FPP) in the brain tissue are believed to play a key role in neurodegeneration;[8] the latter is also linked to the metabolism of phosphorylated tau (P-Tau) protein in the human brain. It is indeed possible that the prenylation cascade from FPP → GGPP → RhoA-cdc42 →GSK3-β → P-Tau is largely (or in part) responsible for Alzheimer's-associated tau phosphorylation and tangle formation of neurons. Elevated levels of P-Tau lead to neurofibrillary tangle formation in the brain, a pathological hallmark of neurodegeneration and the Alzheimer's disease (AD). In this study, we report a genetic relationship between hFPPS and P-Tau concentration in the cortical area of the human brain in AD subjects.

The potential value of hFPPS as a therapeutic target (beyond for bone-related diseases) has fuelled efforts toward the identification of nonbisphosphonate inhibitors for this target. Fragment-based screening by NMR and X-ray crystallography led to the first discovery of compounds (e.g. **3**) that could bind in an allosteric pocket of hFPPS near the IPP subpocket.[9] Subsequent optimization of these hits provided nonbisphosphonate allosteric inhibitors with nanomolar potency (e.g., **4**; Figure 1b). More recently, in silico studies identified bisamidine-type inhibitors with micromolar potency;[10] however, the binding of these molecules in the allosteric pocket has not been confirmed. In this report, we describe the discovery of thienopyrimidine bisphosphonates (ThP-BPs; **6**) that exhibit a mixed binding mode and can interact with both the allylic subpocket of the active site and the allosteric pocket of hFPPS. Structural remodeling of these compounds to the monophosphonate derivatives (ThP-MP; **7**) resulted in a new chemotype of hFPPS inhibitors that bind selectively in the allosteric pocket and exhibit equivalent in vitro potency to compound **4**. In a preliminary biological evaluation, we examined the ability of several, structurally diverse hFPPS inhibitors to modulate intracellular P-Tau levels in human immortalized neurons. Our combined medicinal chemistry efforts and genetic analysis data clearly supports a biochemical link between prenylation and the accumulation of P-Tau in neurons and the AD brain that can potentially be alleviated by inhibiting hFPPS.

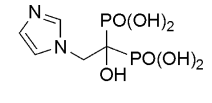

1

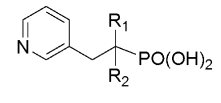

2a, R_1 = $PO(OH)_2$, R_2 = OH
2b, R_1 = $PO(OH)_2$, R_2 = H
2c, R_1 = R_2 = H

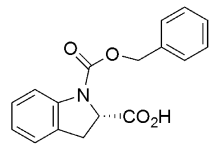

3

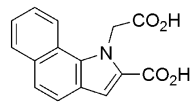

4

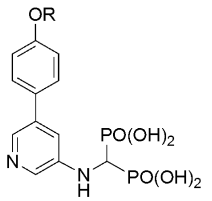

5m, R = isopropyl
5n, R = cyclopropyl

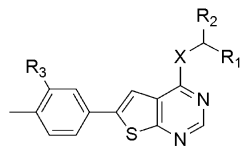

6a, R_1 = R_2 = $PO(OH)_2$, X = NH, R_3 = H
7, R_1 = $PO(OH)_2$, R_2 = H, X = NH, R_3 = H
8, R_1 = $PO(OH)_2$, R_2 = H, X = $NHCH_2$, R_3 = H
9, R_1 = $PO(OH)_2$, R_2 = R_3 = H, X = CH_2
10, R_1 = CO_2H, R_2 = H, X = NH, R_3 = H
11, R_1 = $PO(OH)_2$, R_2 = H, X = NH, R_3 = Cl
12, R_1 = $PO(OH)_2$, R_2 = Ph, X = NH, R_3 = Cl

RESULTS AND DISCUSSION

Screening for Allosteric Inhibitors of hFPPS. The bisphosphonate moiety is a chemically stable bioisostere of pyrophosphate. Mindful of the direct interactions that the pyrophosphate moiety of IPP makes with the positively charged residues in its binding pocket (K57, R60, and R113; Figure 1a,b) and the proximity of these residues to the allosteric pocket, we speculated that in the *absence* of Mg^{2+} ions bisphosphonates may also bind near (or in) the allosteric pocket. The molecular recognition elements surrounding this pocket could conceivably have practical bearings in allowing pyrophosphate-containing metabolites to discriminate between the allylic subpocket and the R/K-rich IPP/allosteric site on the basis of the protein conformation. It is noteworthy that although the biological role of this allosteric pocket is still unknown, on the basis of its amphiphilic nature and proximity to the active site, a regulatory role in feedback inhibition by downstream isoprenoids is plausible and has been proposed.[9] Furthermore, a mixed binding mode of pyrophosphate-containing isoprenoids is not unprecedented; binding of IPP to the allylic subpocket of hFPPS[1b] and of DMAPP in the IPP subpocket of FPPS from *Trypanosoma cruzi* (PDB ID: 1YHL)[11] have been previously reported.

In earlier studies, we reported the synthesis and in vitro activity of aminopyridine-based bisphosphonate (*N*-BP; **5**) and thienopyrimidine-based bisphosphonate (ThP-BP; **6**) inhibitors of hFPPS (Table 1).[12] In this study, we investigated their binding to hFPPS using differential scanning fluorimetry (DSF). The thermal unfolding of hFPPS (ΔT_m) in the presence and absence of these ligands was compared to their in vitro potency (Figures 2 and 3). Initial validation of our DSF assay was carried out with a number of control experiments using known compounds. For example, the DSF data of the hFPPS/**2a** and hFPPS/**2a**/IPP complexes (ΔT_m of 22 ± 0.5 and 30 ± 0.5 °C, respectively) were found to be consistent with literature DSC data.[1a] Additionally, the thermal stability of the hFPPS/**4** complex (ΔT_m = 8 ± 0.5 °C) was found to be lower than that of hFPPS/**2a** and invariable by the presence or absence of IPP and Mg^{2+} ions. These observations are in

dx.doi.org/10.1021/jm500629e | J. Med. Chem. 2014, 57, 5764−5776

Table 1. Library of hFPPS Inhibitors Used for Screening: *N*-BPs and ThP-BPs with General Structure 5 and 6, Respectively (The Synthesis of These Compounds Were Previously Reported[12])

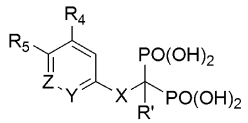

5a, R_4 = **a**, R_5 = H, X = CH_2, Y = CH, Z = N, R' = Fluorine
5b, R_4 = **a**, R_5 = H, X = CH_2, Y = CH, Z = N, R' = H
5c, R_4 = **a**, R_5 = H, X = NH, Y = CH, Z = N, R' = H
5d, R_4 = **a**, R_5 = H, X = NH, Y = N, Z = CH, R' = H
5e, R_4 = H, R_5 = **a**, X = NH, Y = N, Z = CH, R' = H
5f, R_4 = **b**, R_5 = H, X = NH, Y = N, Z = CH, R' = H
5g, R_4 = **c**, R_5 = H, X = NH, Y = CH, Z = N, R' = H
5h, R_4 = **e**, R_5 = H, X = NH, Y = N, Z = CH, R' = H
5i, R_4 = **f**, R_5 = H, X = NH, Y = N, Z = CH, R' = H
5j, R_4 = **h**, R_5 = H, X = NH, Y = N, Z = CH, R' = H
5k, R_4 = **i**, R_5 = H, X = NH, Y = N, Z = CH, R' = H
5l, R_4 = **j**, R_5 = H, X = NH, Y = CH, Z = N, R' = H
5m, R_4 = **j**, R_5 = H, X = NH, Y = N, Z = CH, R' = H
5n, R_4 = **k**, R_5 = H, X = NH, Y = CH, Z = N, R' = H
5o, R_4 = **k**, R_5 = H, X = NH, Y = N, Z = CH, R' = H
5p, R_4 = **l**, R_5 = H, X = NH, Y = N, Z = CH, R' = H
5q, R_4 = **m**, R_5 = H, X = NH, Y = N, Z = CH, R' = H
5r, R_4 = **o**, R_5 = H, X = NH, Y = CH, Z = N, R' = H
5s, R_4 = **p**, R_5 = H, X = NH, Y = CH, Z = N, R' = H
5t, R_4 = **q**, R_5 = H, X = NH, Y = CH, Z = N, R' = H
5u, R_4 = **r**, R_5 = H, X = NH, Y = N, Z = CH, R' = H

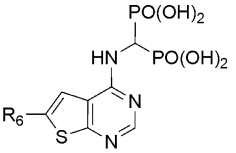

6a, R_6 = **d**
6b, R_6 = **g**
6c, R_6 = **h**
6d, R_6 = **i**
6e, R_6 = **j**
6f, R_6 = **k**
6g, R_6 = **n**
6h, R_6 = **o**

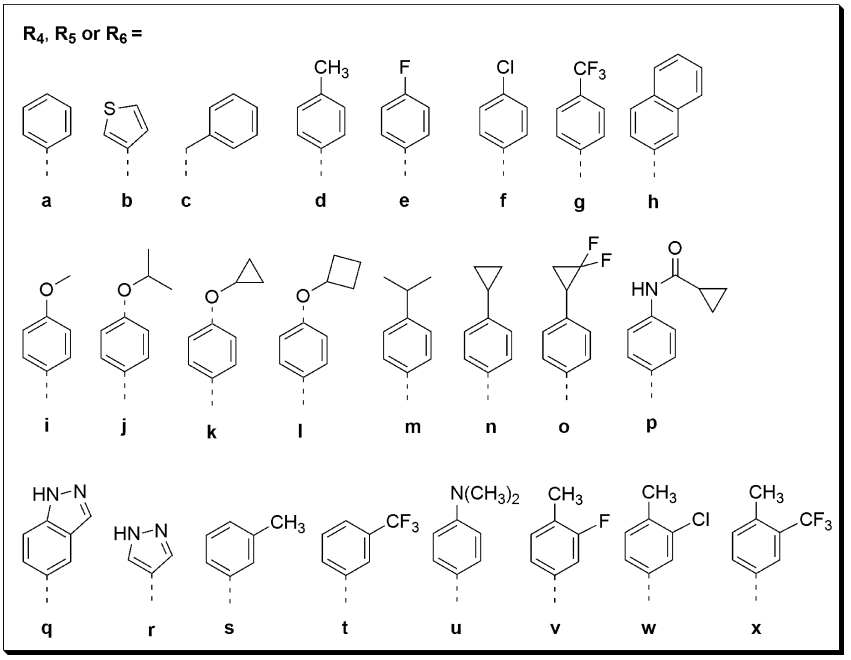

agreement with the lower intrinsic potency of **4** (compared to **2a**) and its competitive binding with IPP.[9]

A number of hFPPS/**5** and hFPPS/**6** complexes were then evaluated by DSF in the presence and absence of the enzyme's Mg^{2+} cofactor (Table 1; Figure 3). To minimize the impact of false positive hits due to nonselective binding, only inhibitors with IC_{50} values below 2 μM and selectivity >100-fold for inhibiting hFPPS vs hGGPPS were included in this screen (Figure 2); *N*-BPs are known to inhibit related enzymes, such as hGGPPS[13] and hSQS.[14] In the presence of Mg^{2+} ions, a good correlation between the ΔT_m and IC_{50} values for the *N*-BPs (**5**) was observed (Figure 3a). Predictably, in the absence of Mg^{2+} ions binding was virtually abolished (ΔT_m <2 °C ± 0.5 °C). Exceptionally, few complexes (e.g. hFPPS/**5n**), exhibited thermal stability that was 3−4 °C higher than the unliganded enzyme. In general, the hFPPS/**6** complexes exhibited higher thermal stability than the hFPPS/**5** complexes in both the presence and absence of Mg^{2+} ions (albeit fewer ThP-BPs were tested). Under Mg^{2+}-free conditions, several hFPPS/**6** complexes exhibited thermal stability equivalent to that of the hFPPS/**4** complex (Figure 3b).

To further characterize the binding of our compounds in the presence and absence of Mg^{2+} ions, competitive binding between pairs of ligands was investigated using ^1H line broadening NMR. Broadening of the ^1H resonances of inhibitor **4** was observed in the presence of Mg^{2+} ions and hFPPS (Supporting Information Figure 1), suggesting fast exchange between the free and enzyme-bound state of **4**. Addition of **2a**

dx.doi.org/10.1021/jm500629e | J. Med. Chem. 2014, 57, 5764−5776

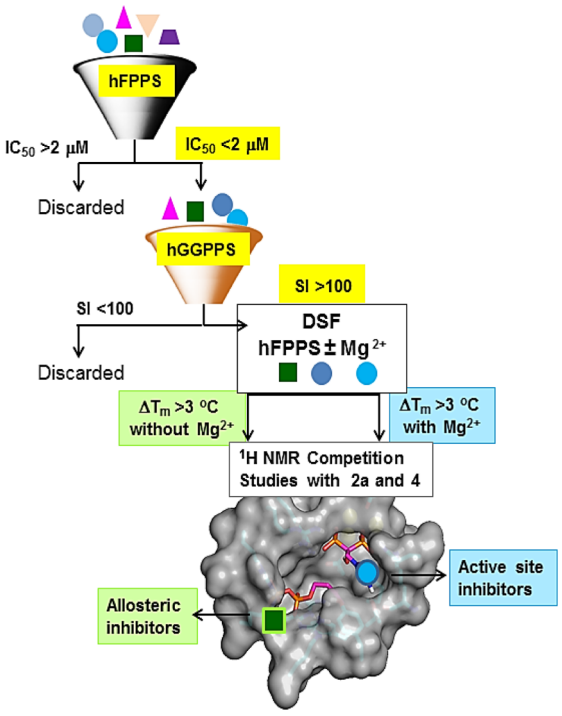

Figure 2. Screening protocol (SI, selectivity index = potency ratio in hFPPS/hGGPPS).

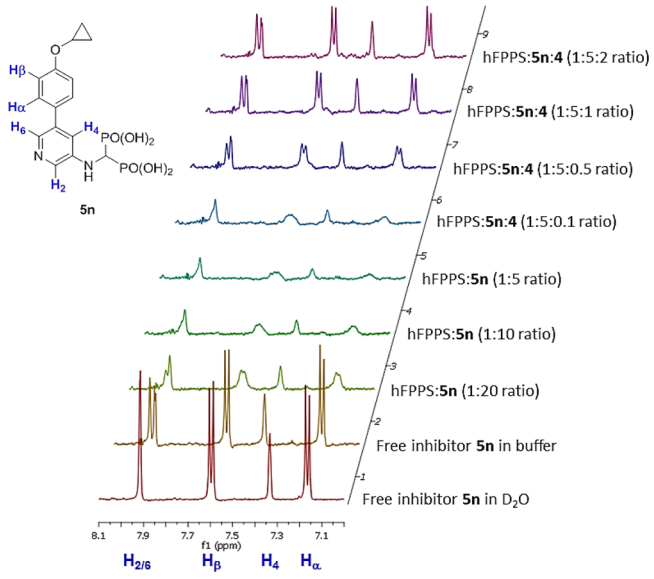

Figure 4. ^{1}H line broadening NMR studies exploring competitive binding of inhibitors **4** and **5n** in the absence of Mg^{2+} ions. Stacked spectra of compound **5n** free in solution (D_2O and buffer) and in the presence of hFPPS and **4**; for clarity, only the aromatic resonances are shown, the molar ratio of ligands and protein are indicated next to each spectra and the proton resonances of **5n** are indicated at the bottom of the stacked spectra (in blue).

to the same NMR sample did not restore the ^{1}H resonances of **4** (Supporting Informationm Figure 1), indicating that **2a** and **4** do not compete for binding to hFPPS. This is in complete agreement with the structure of the hFPPS/**1**/**3** ternary complex (PDB ID: 3N46), which demonstrated that the allosteric pocket and the allylic subpocket can be simultaneously occupied.[9] In contrast, competitive binding was detected between **4** and IPP (Supporting Information Figure 2), consistent with the expected electrostatic/steric clash between one carboxylic acid moiety of **4** and the pyrophosphate of IPP (PDB ID: 3N6K).[9] In the absence of Mg^{2+} ions, our NMR data clearly showed competitive binding between inhibitors **5n** and **4** (Figure 4). However, in the presence of Mg^{2+} ions, the data was inconclusive and we could not rule out that **5n** was competing for binding with both **2a** and **4**; similar observations were made with analogue **6a**.

Co-crystallization of **6a** bound to hFPPS in both the presence and absence of Mg^{2+} ions provided proof that this compound can bind to both the allylic subpocket of the active site and the allosteric pocket (Figure 5). ThP-BP **6a** is the first chemotype to provide conclusive evidence that bisphosphonates can indeed bind in the allosteric pocket of hFPPS, at least in the absence of the metal cofactor. From here on, we will refer to hFPPS/**6** complexes as the hFPPS/**6**$^{(act)}$ and hFPPS/**6**$^{(allo)}$ complexes to indicate binding of the ligand in the active site and allosteric pocket, respectively (part a vs part b of Figure 5; PDB IDs 4JVJ vs 4LPG, respectively).

We previously reported the co-crystal structure of the hFPPS/**6a**$^{(act)}$ complex (PDB ID 4JVJ; Figure 5a).[12d] In the hFPPS/**6a**$^{(allo)}$ complex, the *p*-tolyl substituent is buried in the allosteric pocket, engaging in π-stacking interactions with the side chains of N59 and F206 (Figure 5b). The alkyl portions of the L344 and K347 side chains are within van der Waals radius and provide additional hydrophobic interactions. Edge-to-face π-stacking interactions are also observed between the thienopyrimidine core and F239, with the pyrimidine ring partially solvent exposed (Figure 5b). A noteworthy difference in the allosteric bindings of **6a** and **4** is that **4** engages in direct

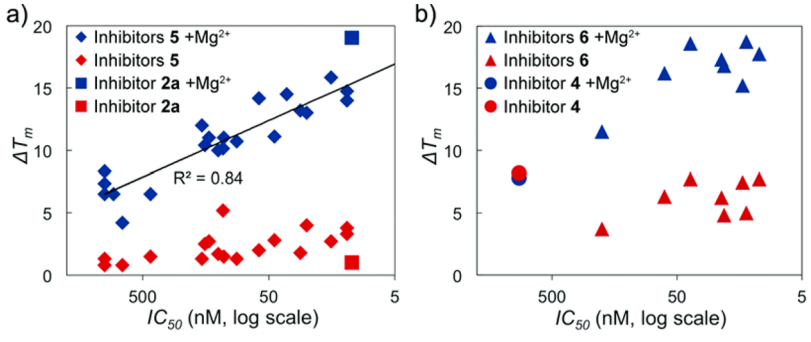

Figure 3. Correlation of in vitro potency in inhibiting hFPPS to the thermal stability of the hFPPS/inhibitor complex in the presence and absence of Mg^{2+} ions. DSF assays were run with 4 mM hFPPS protein and 40 mM inhibitor. (a) IC_{50} vs ΔT_m of hFPPS/*N*-BP complexes. (b) IC_{50} vs DTm of hFPPS/ThP-BP and hFPPS/**4** complexes.

dx.doi.org/10.1021/jm500629e | J. Med. Chem. 2014, 57, 5764−5776

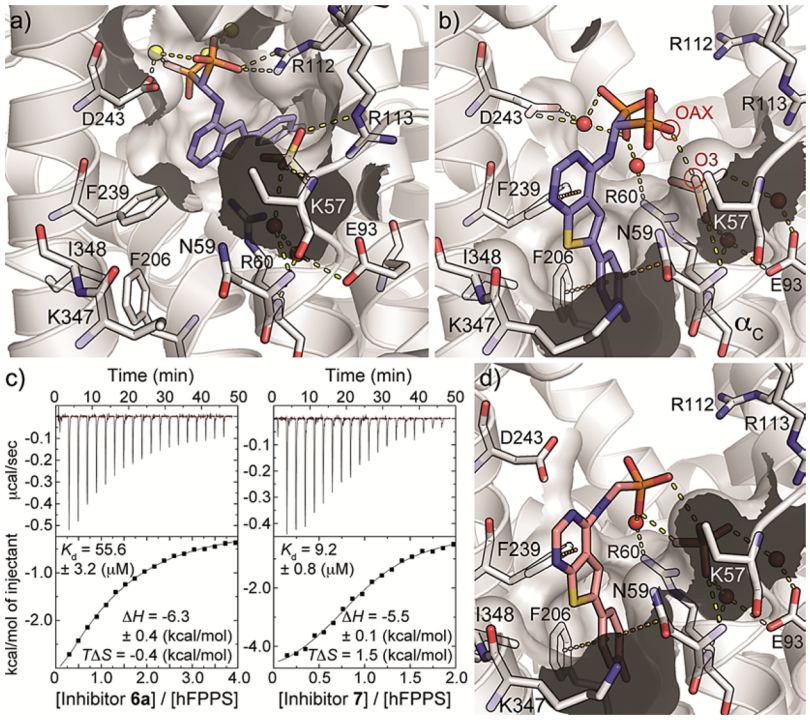

Figure 5. Co-crystal structures of hFPPS/ligand complexes. (a) Complex hFPPS/**6a**$^{(act)}$/Pi (PDB ID: 4JVJ); metal-coordinated water molecules and some other interactions between the protein and the inhibitor are omitted for clarity. (b) Complex hFPPS/**6a**$^{(allo)}$/Pi (PDB ID: 4LPG). (c) ITC data for the binding of compounds **6a** and **7** in the absence of Mg^{2+} ions. (d) Structure of the hFPPS/**7**/Pi complex (PDB ID: 4LPH).

interactions with the side chains of K57 and R60 via one of its carboxylic acids, whereas the bisphosphonate of **6a** does not form any direct interaction but only water-mediated H-bonds with R60 and D243; the latter residue (D243) is typically involved in metal-mediated interaction with bisphosphonates that are bound in the allylic subpocket (part a vs part b of Figure 5). Surprisingly, the bisphosphonate of **6a** is bound very close to an inorganic phosphate ion (Pi) occupying the IPP subpocket (a distance of 2.64 Å between OAX and O3; Figure 5b). Although such proximity between two negatively charged ions is puzzling, the identity and location of both was unambiguously confirmed by anomalous scattering data (Supporting Information Figure 3). Presumably, the negative charge of the Pi is neutralized by the dipole of the α_C helix and/or R60 (a distance of 3.15 Å was observed between a guanidinium nitrogen and a phosphate oxygen).

The relative contributions of the two binding modes of **6a** under biologically relevant conditions are difficult to decipher. Whether they both contribute to the intrinsic potency of **6a** (IC_{50} = 22 nM) is equally unclear; in vitro evaluation of hFPPS activity requires Mg^{2+} as the cofactor, which biases the binding of bisphosphonates in favor of the allylic subpocket. Nonetheless, under Mg^{2+}-free conditions, ITC studies suggested a K_d of ~56 µM for the binding of **6a**, presumably in the allosteric pocket only (Figure 5c). The K_d of the corresponding *mono*-phosphonate analogue **7** was ~9 µM and in close agreement with its IC_{50} value of 4.5 µM (Table 2). More importantly, in the presence of Mg^{2+} ions, competitive binding of **7** was unambiguously observed with compound **4** but not with **2a**. These results suggest that under biologically relevant conditions inhibitor **7** binds selectively in the allosteric pocket (Figure 6). It is noteworthy that previous attempts to remove one of the phosphonate moieties of *N*-BPs led to complete loss of potency (e.g., **2b** vs **2c**; Table 2).[15]

Table 2. Inhibition Data for Key Compounds

compd	hFPPS[a] IC_{50} (µM)	P-Tau/T-Tau[e] ratio	LDH[f] (%)
control		0.012	0
1	0.003	0.006	+60
2a	0.006	0.004	+60
2b	0.033[b]	nd	nd
2c	>800[b]	nd	nd
4	0.92[c]	0.004	+3
5n	0.018	0.007	0%
6a	0.022	nd	nd
6f	0.014	0.009	−1
7	4.5	nd	nd
8	>20[d]	nd	nd
9	26	nd	nd
10	>20[d]	nd	nd
11	3.3	nd	nd
12	1.2	0.010	−7

[a]The potencies of all analogues of general structure **5** and **6** in inhibiting hFPPS were previously reported.[12] [b]IC_{50} reported by Dunford et al.[15] [c]IC_{50} of 0.2 µM was reported by Jahnke et al. using a different assay protocol.[9] [d]Inhibition of 40% and 27% was observed for **8** and **10**, respectively, at 20 µM. [e]P-Tau/T-Tau ratios in human neuroblastoma SH-SY5Y cells were determined at a fixed concentration of 100 nM inhibitor after an incubation period of 24 h; average value of two assays; deviation of <5% was observed. [f]Average % activity of lactate dehydrogenase observed (LDH) compared to the untreated control (set arbitrarily to zero LDH activity); assays run in triplicate and a standard deviation of ~10% was observed.

We subsequently confirmed the binding of **7** in the allosteric pocket by X-ray crystallography (Figure 5d). The overall structures of the hFPPS/**7** and hFPPS/**6a**$^{(allo)}$ complexes are very similar, with the core (Cα) rmsd value of 0.27 Å. Alignment of the two structures showed clear superposition of

dx.doi.org/10.1021/jm500629e | J. Med. Chem. 2014, 57, 5764−5776

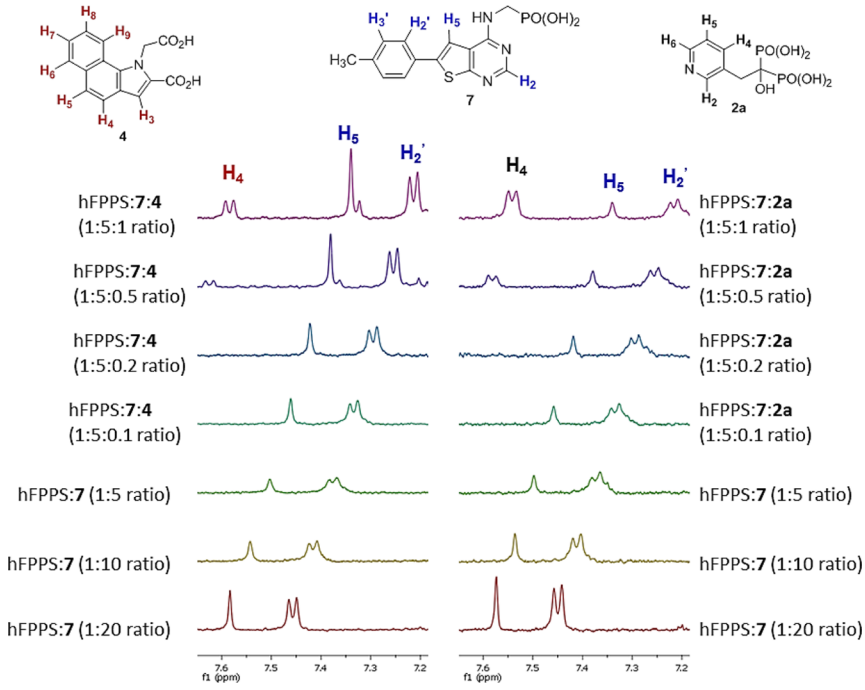

Figure 6. Side-by-side comparison of ^{1}H line broadening NMR studies exploring competitive binding of hFPPS inhibitor **7** with either **4** or **2a** in the *presence* of Mg^{2+} ions. Buffer: BSA 20 mg/mL, Tris 50 mM, pH 7.7, $MgCl_2$ 2 mM, TCEP 0.5 mM. For clarity, only select regions of the spectra are shown; the molar ratio of ligands and protein are indicated next to each spectra. Stacked spectra on the left are those of compound **7** free in solution and in the presence of hFPPS and compound **4**; the data clearly shows competitive binding even in the presence of Mg^{2+} ions. Stacked spectra on the right are those of compound **7** free in solution and in the presence of hFPPS and compound **2a**, clearly showing that binding of the two compounds is not competitive in the presence of Mg^{2+} ions. All proton resonances are labeled at the top of the spectra in red, blue, and black for compounds **4**, **7**, and **2a**, respectively.

the thienopyrimidine cores, the tolyl side chains and the Pi (part b vs part d of Figure 5). Although the phosphonate moiety of **7** did not overlap with either of the two phosphonates of **6a**, it maintained a water-mediated interaction with R60. In an attempt to gain more insight as to the importance of this phosphonate moiety, and possibly allow this moiety to form a direct salt-bridge with R60, we synthesized analogue **8**, having a longer linker between the phosphonate and the thienopyrimidine core. A significant drop in potency was observed (Table 2), likely due to the increased conformational freedom and entropic penalty associated with the binding of **8**. We also investigated the impact of decreasing the acidity of this pharmacophore by replacing the exocyclic NH with a methylene linker at C-4 (pK_a of P(O)O$^-$OH of ∼6.8 and ∼7.7 for analogues **7** and **9**, respectively) and by completely replacing the phosphonate with a carboxylic acid moiety (i.e., **10**). A correlation between loss in potency and decrease in the acidity of this moiety was clearly observed, confirming the importance of this pharmacophore (Table 2). Finally, minor substitutions on the tolyl side chain (e.g., **11**; IC_{50} = 3.3 μM) and the Cα to the phosphonate were well tolerated and appear to be additive in improving the potency of this class of compounds. In the present study, analogue **12** (IC_{50} = 1.2 μM) was the most potent hit identified, exhibiting equivalent potency to compound **4** in inhibiting hFPPS in our in vitro assay (IC_{50} = 0.92 μM). More extensive SAR investigations and further optimizing of these allosteric inhibitors is currently in progress.

Synthesis of Ligands Binding to the Allosteric Pocket. The synthesis of the new compounds **7**−**12** was initiated from the key intermediate **13**, prepared as previously reported.[16] Treatment of **13** first with Br_2 in acetic acid, followed by $POCl_3$, provided the 4-chloro-6-bromo intermediate **14** in moderate overall yield (∼40% over the two steps). Analogues **7**, **11**, and **12** were prepared after sequential S_NAr displacement of the C-4 chloro with an aminodiethylphosphonate (prepared as previously reported[17]), followed by Suzuki cross-coupling with an aryl boronate and final deprotection of the phosphonate esters with TMSBr/MeOH (Scheme 1). Alternatively, the Suzuki reaction could be carried first to obtain the key building block 4-chloro-6-(*p*-tolyl)thieno[2,3-*d*]pyrimidine, followed by the S_NAr displacement of the C-4 chloro with diethyl (2-aminoethyl)phosphonate to give the diethyl ester of analogue **8**, or the unprotected glycine to obtain directly compound **10**, with similar overall yields. These two alternative approaches provide easy access to library synthesis of analogues with structural diversity at both the C-4 and C-6 of the thienopyrimidine scaffold.

Suzuki−Miyaura cross coupling of trifluoro(vinyl) borane with the 4-chlorothienopyrimidine, followed by modified Lemieux−Johnson oxidation,[18] gave the aldehyde **15** in good overall yields (Scheme 1). Horner−Wadsworth−Emmons type condensation of intermediate **15** with the sodium anion of tetraethyl methylenediphosphonate gave the α,β-unsaturated monophosphonate diethyl ester.[19] Attempts to remove the ethyl esters of this intermediate (under the usual condition of TMSBr/MeOH) led to some decomposition, therefore, this intermediate was first hydrogenated before the deprotection step to give compound **9** (Scheme 1).

Relevance of hFPPS in Modulating Phospho-Tau Levels in the Human Brain. Elevated plasma cholesterol levels are known among the vascular risk factors of the

dx.doi.org/10.1021/jm500629e | J. Med. Chem. 2014, 57, 5764−5776

Scheme 1. Synthesis of Allosteric Inhibitors of hFPPS[a]

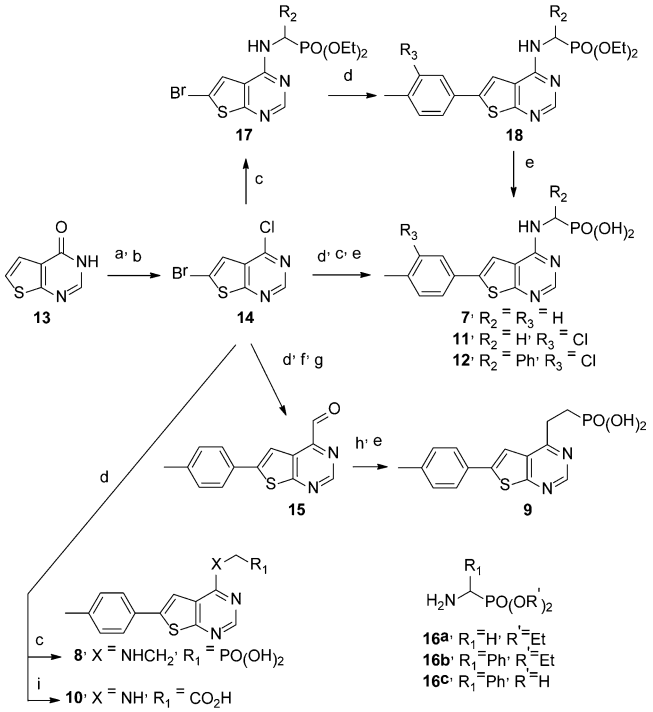

[a]Conditions: (a) Br_2, AcOH, 80 °C (63%); (b) $POCl_3$, 95 °C (58%); (c) $H_2NCHR_1PO(OR')_2$ (**16**), Et_3N, dioxane, 100 °C, 18−24 h (40−60%); (d) $Pd(PPh_3)_4$, K_2CO_3, dioxane/H_2O (1:1), 100 °C, 1 h (60−70%); (e) TMSBr, MeOH, RT, 72 h (>98% conversion, 50−80% isolated yield); (f) potassium trifluoro(vinyl)borate, $PdCl_2(dppf)$-CH_2Cl_2, Et_3N, *i*-PrOH/H_2O, 100 °C, 1 h (72%); (g) (i) OsO_4, NMO, 2,6-lutidine, acetone/H_2O, RT, 2 h, (ii) $NaIO_4$, RT, 1 h (64%); (h) (i) tetraethyl methylenediphosphonate, NaH, THF, 0 °C to RT, 1 h, (ii) H_2, Pd/C, RT, 1 h, then step e (45% isolated yield for the 3 steps); (i) $H_2NCH_2CO_2H$, Na_2CO_3, dioxane/H_2O (1:1), 100°C, 3 h (60%).

Alzheimer's disease (AD).[20,21] Although not a universal finding, treatment of middle-aged individuals for hypercholesterolemia with statins has been shown to confer some level of neuroprotection against late-life development of AD.[22] Additionally, statin treatment has been shown to reduce the cerebrospinal fluid phospho-tau content in the human brain.[23] These finding are consistent with the quasi-absence of cortical neurofibrillary tangles in autopsy-confirmed cognitively intact subjects who had used statins for several years as opposed to nonusers.[24]

Phospho-tau production in the brain is regulated by a select number of isoprenoid-activated small G proteins that control the function of the GSK3-β kinase. GSK3-β is believed to be responsible for high levels of tau phosphorylation in neurons.[25] This hypothesis prompted us to carefully examine the relationship between the hFPPS gene and tau metabolism in the Alzheimer's disease (AD).[26] We examined a cohort of 751 pairs of AD and age-matched control subjects to map approximately 535000 polymorphisms in each of the AD cases and control subjects. Five single nucleotide polymorphisms (SNPs) were examined in the hFPPS gene loci (Supporting Information Figure 4). Frontal cortex brain samples (n = 116) from autopsy-confirmed cases of Alzheimer's disease and age-matched control subjects were prepared according to an established protocol[27] prior to ELISA quantification of cortical total tau (T-Tau) and phosphorylated tau (P-Tau) protein levels. While none of the markers were found to exhibit significant association with sporadic AD, a specific and dose dependent genetic association was found between variant rs4971072 (SNP:A/G) in the promoter region of the hFPPS gene and P-Tau protein levels ($p < 0.02$) in the cortical area of the AD brain (Figure 7a). We also examined a subset of AD (n = 34) and age-matched control brains (n = 24) for the mRNA prevalence of hFPPS using QrtPCR as previously reported.[28] Human FPPS mRNA levels were markedly elevated in the cortical cortices of the AD versus the control subjects (Figure 7b), consistent with a hyperactivation of the isoprenoid pathway in Alzheimer's disease. Although these finding do not imply that hFPPS is causally related to Alzheimer's disease, they support a genetic association between specific genetic variants in hFPPS (rs4971072) and the P-Tau concentrations in the human AD brain. One of the early pathological features of common Alzheimer's disease is the progressive accumulation of ribbon-like intraneuronal tangles made of polymer of the phosphorylated tau protein (P-Tau), a key cytoskeleton structural component of neurons. Human FPPS clearly affects the accumulation of the pro-toxic P-Tau and may accelerate the progression of AD pathology.[26]

These preliminary results prompted us to also examine the ability of hFPPS inhibitors to block tau metabolism in human neuroblastoma SH-SY5Y cells. Cells were treated with both bisphosphonate and nonbisphophonate inhibitors at concentrations of 100 and 500 nM for a period of 24 h before they were lysed and their T-Tau and P-Tau levels were quantified using an established ELISA test.[27] Toxicity to the neurons was

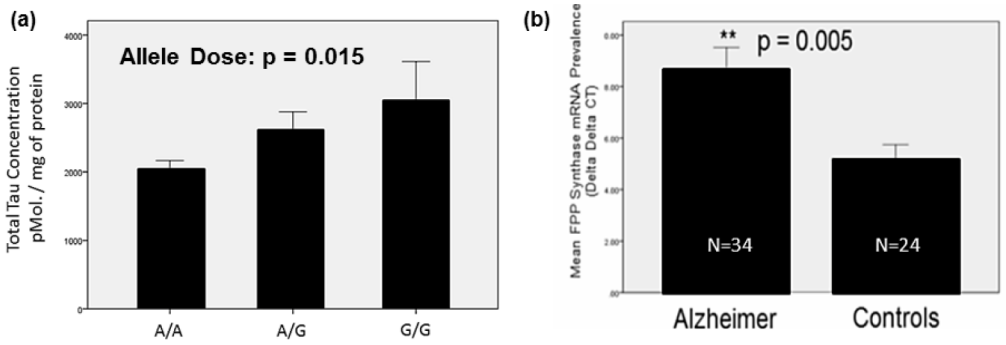

Figure 7. Genetic association between hFPPS and P-Tau metabolism. (a) Effects of rs4971072 variant copy number on P-Tau concentrations in cortical area of the AD brain. (b) Human cortical FPPS mRNA prevalence in the cortical area in AD brain vs control. AD mean Braak stage = 4.9 ± 1.8; age of AD onset = 71 ± 10; age of death = 74 ± 12 and 78 ± 9 for control and AD, respectively.

dx.doi.org/10.1021/jm500629e | J. Med. Chem. 2014, 57, 5764−5776

estimated using a routine lactate dehydrogenase (LDH) assay and found to increase sharply after 48 h of incubation with the inhibitors tested. Similarly, some toxicity was observed with most inhibitors if tested at concentrations of 500 nM or higher, prohibiting a clear determination of P-Tau/T-Tau levels. Although a significant decrease (≥50% decrease) in the P-Tau/T-Tau levels was observed with the most potent *N*-BP inhibitors **1** and **2a**, significant toxicity was also observed (~60% higher LDH activity as compared to the untreated control) even at concentrations of 100 nM (Table 2). In contrast, the bisphosphonate inhibitors **5n** and **6f** and nonbisphosphonate inhibitor **4** induced a significant decrease in P-Tau/T-Tau ratio without significant toxicity, whereas the monophosphonate inhibitor **12** exhibited only minor effects (Table 2).

CONCLUSIONS

In our search for allosteric inhibitors of hFPPS, we screened a small library of bisphosphonates using a multistage biochemical and structural platform. Mindful of the structural features of the allosteric pocket, we anticipated that binding in this pocket of large lipophilic bisphosphonates may be possible, particularly in the absence of Mg^{2+} ions. These studies led to the identification of thienopyrimidine-based monophosphonate allosteric inhibitors. Our screening protocol was guided by DSF, ITC, ^{1}H line-broadening NMR, and X-ray crystallography in the presence and absence of the enzyme's metal cofactor. We also characterized the binding interactions between the hFPPS allosteric pocket and the bisphosphonate inhibitor **6a** and compared them to those observed with the selective allosteric inhibitor **7**. The protein−ligand interactions observed in both complexes were virtually identical, thus validating screening hFPPS under Mg^{2+}-free conditions. Although Mg^{2+}-free conditions are not biologically relevant, this approach proved to be useful for screening hFPPS and may be applicable to other structurally/functionally related targets. Recently, a similar three-stage biophysical screening method was reported as a general tool for screening in fragment-based drug discovery.[29]

In addition, analysis of our collective X-ray data on thienopyrimidine-based inhibitor bound in the allylic subpocket and the allosteric pocket (e.g., **6a**$^{(act)}$ vs **6a**$^{(allo)}$; PDB codes 4JVJ and 4LPG, respectively) revealed very similar interactions involved in both binding sites. For example, the π-stacking interactions between the tolyl side chain of **6a** and Phe99/Gln171 in the hFPPS/**6a**$^{(act)}$ complex are analogous to those observed in the hFPPS/**6a**$^{(allo)}$ complex with Phe206/Asn59 (Figure 5b). This finding is intriguing and supports the hypothesis that the allosteric pocket plays a regulatory role in product feedback inhibition that is sensitive to the concentration of isoprenoids and independent of the Mg^{2+} cofactor concentration.

We identified thienopyrimidine-based monophosphonates (ThP-MP) as a new chemotype of hFPPS allosteric inhibitors. These compounds are amenable to further optimization and may provide tools for validating hFPPS as a therapeutic target for nonskeletal diseases such as various cancers and neurodegenerative diseases. A relationship between the latter and the levels of FPP/GGPP in the human brain has been previously reported.[8] Herein we provide further evidence of a genetic link between hFPPS and the levels of phosphorylated tau (P-Tau) in the human AD brain. The accumulation of P-Tau in the brain is associated with the pathological accumulation of neurotoxic neurofibrillary tangles, an established hallmark of AD brain pathology. Preliminary evaluation of hFPPS inhibitors in neuroblastoma cells suggested that hFPPS can modulate tau metabolism; confirmation of these results is pending the identification of more potent/less toxic inhibitors of hFPPS with good cell-membrane permeability. Nonetheless, our collective data supports further investigation of hFPPS as a potential therapeutic target for decelerating the progression of AD and other tauopathy-related neurodegenerative diseases.

EXPERIMENTAL SECTION

General Procedures for Characterization of Compounds. All compounds were purified by normal phase flash column chromatography on silica gel using a CombiFlash instrument and a solvent gradient from 5% EtOAc in hexanes to 100% EtOAc and then to 20% MeOH in EtOAc, unless otherwise indicated. The homogeneity of all final compounds (**7**−**12**) was confirmed to ≥95% by reverse-phase HPLC. Only phosphonate esters with homogeneity ≥95% were processed further to the final phosphonic acid inhibitors **7**−**9**, **11**, and **12**. HPLC analysis was performed using a Waters ALLIANCE instrument (e2695 with 2489 UV detector and 3100 mass spectrometer). Each final compound was fully characterized by ^{1}H, ^{13}C, and ^{31}P NMR and HRMS. Chemical shifts (δ) are reported in ppm relative to the internal deuterated solvent (^{1}H, ^{13}C) or external H_3PO_4 (δ 0.00 ^{31}P), unless indicated otherwise. The high-resolution MS spectra of final products were recorded using electrospray ionization (ESI$^{\pm}$) and Fourier transform ion cyclotron resonance mass analyzer (FTMS). Method (homogeneity analysis using a Waters Atlantis T3 C18 5 μm column): solvent A, H_2O, 0.1% formic acid; solvent B, CH_3CN, 0.1% formic acid; mobile phase, linear gradient from 95%A and 5%B to 5%A and 95%B in 13 min, then 2 min at 100% B; flow rate, 1 mL/min.

General Synthetic Protocols. Suzuki cross-coupling reactions and deprotection of the diethyl phosphonates to the phophonic acids were carried out using the general protocols previously reported.[12]

General Protocol for S_NAr displacement of the C-4 Chloro. For the preparation of inhibitors **7**, **11**, and **12**, this reaction was carried out using the 4-cholo intermediate **14**, whereas for the synthesis of inhibitors **8** and **10**, this reaction was carried out using the common building block 4-chloro-6-(*p*-tolyl)thieno[2,3-*d*]pyrimidine (formed after Suzuki cross-coupling of the 4-tolylboronic acid with **14**). In a pressure vessel, the 4-chlorothienopyrimidine was dissolved in dioxane, the amine reagent (aminophosphonate; 1.5 equiv) and Et_3N (5 equiv) were added, and the pressure vessel was sealed. The reaction mixture was stirred at 100 °C for 15−24 h; completion of the reaction was monitored by HPLC. The reaction mixture was cooled to RT and diluted with ethyl acetate (50 mL). The organic layer was washed with an aqueous solution of saturated $NaHCO_3$ (15 mL), water (45 mL), and brine (15 mL) and dried over anhydrous $MgSO_4$. The crude was purified by column chromatography to give the desired products. The same procedure was used for the synthesis of compound **10**, however, the solvent was changed to dioxane:H_2O (1:1) and Na_2CO_3 (1.5 equiv) was used as the base; the reaction was completed in 3 h.

*(((6-(p-Tolyl)thieno[2,3-d]pyrimidin-4-yl)amino)methyl)-phosphonic Acid (**7**).* The final compound **7** was isolated as a white powder (7.4 mg, 50% isolated yield). ^{1}H NMR (500 MHz, D_2O, 5% ND_4OD) δ 7.92 (s, 1H), 7.35 (s, 1H), 7.21 (d, J = 8.0 Hz, 2H), 6.90 (d, J = 8.0 Hz, 2H), 3.29 (d, J = 13.3, 2H), 2.10 (s, 3H). ^{13}C NMR (126 MHz, D_2O, 5% ND_4OD) δ 162.5, 156.4 (d, J = 9 Hz), 152.4, 140.0, 138.8, 129.6, 129.3, 125.2, 118.3, 113.2, 40.4 (d, J = 135 Hz), 20.4. ^{31}P NMR (202 MHz, D_2O, 5% ND_4OD): δ 12.96. HRMS (ESI$^-$) m/z 334.0415 calculated for $C_{14}H_{13}N_3O_3PS$; found m/z 334.0420 $[M - H]^-$.

*(2-((6-(p-Tolyl)thieno[2,3-d]pyrimidin-4-yl)amino)ethyl)-phosphonic Acid (**8**).* The diethyl ester of inhibitor **8** was isolated as a brown solid (45.8 mg, 59% yields). ^{1}H NMR (500 MHz, CD_3OD) δ 8.29 (s, 1H), 7.57 (s, 1H), 7.51 (d, J = 8.0 Hz, 2H), 7.21 (d, J = 8.0 Hz, 2H), 4.13−4.09 (m, 4H), 3.83−3.77 (m, 2H), 2.34 (s, 3H), 2.31−

dx.doi.org/10.1021/jm500629e | J. Med. Chem. 2014, 57, 5764−5776

2.24 (m, 2H), 1.31 (t, J = 7.1 Hz, 3H). ^{13}C NMR (126 MHz, CD_3OD) δ 164.0, 156.5, 153.0, 140.4, 138.6, 130.5, 129.4, 125.5, 118.1, 112.7, 62.0 (d, J = 6.5 Hz), 34.6 (d, J = 2.1 Hz), 24.6 (d, J = 138.0 Hz), 19.8, 15.3 (d, J = 6.1 Hz). ^{31}P NMR (81 MHz, CD_3OD) δ 30.33. MS (ESI +) m/z 405.90 $[M + H]^+$ for $C_{19}H_{25}N_3O_3PS$. The final inhibitor **8** was obtained as a light-brown solid (26.2 mg, near quantitative yield). ^{1}H NMR (500 MHz, D_2O, 5% ND_4OD) δ 7.92 (s, 1H), 7.14 (d, J = 8.0 Hz, 2H), 7.09 (s, 1H), 6.88 (d, J = 8.0 Hz, 2H), 3.50−3.45 (m, 2H), 2.13 (s, 3H), 1.76−1.73 (m, 2H). ^{13}C NMR (126 MHz, D_2O, 5% ND_4OD) δ 162.4, 155.6, 152.2, 139.9, 138.6, 129.4, 129.2, 124.9, 118.0, 112.9, 37.7, 29.2 (d, J = 126 Hz), 20.4. ^{31}P NMR (202 MHz, D_2O, 5% ND_4OD): δ 18.5. HRMS (ESI−) m/z 348.0577 calculated for $C_{15}H_{15}N_3O_3PS$; found m/z 348.0569 $[M - H]^-$.

*(2-(6-(p-Tolyl)thieno[2,3-d]pyrimidin-4-yl)ethyl)phosphonic Acid (**9**).* A solution of tetraethyl methylenediphosphonate (26 μL, 0.104 mmol) in THF (3 mL) was cooled to 0 °C, and NaH (60%, 5 mg, 0.125 mmol) was added in a portion and then stirred at 0 °C for 15 min. A solution of aldehyde **15** (29 mg, 0.114 mmol) in THF (1 mL) was added, and the reaction mixture was stirred at RT for 1 h. The reaction was quenched with H_2O, diluted with EtOAc (100 mL), and extracted with 1 N HCl solution (50 mL) and brine (100 mL). The organic layer was collected, dried over $MgSO_4$, concentrated, and purified by chromatography on silica gel (solvent gradient from 0% to 100% EtOAc in Hex). The isolated product was dissolved in EtOH (3 mL), 10% Pd/C (5 mg) was added, and the reaction mixture was stirred under an atmosphere of H_2 for 1 h. The reaction mixture was filtered through Celite and washed with MeOH. The filtrate was concentrated to isolate the product. The isolated product was redissolved in DCM (3 mL) and TMSBr (150 μL, 0.127 mmol) was added dropwise. The reaction mixture was stirred at RT overnight. Subsequently, MeOH (2 mL) was added to the reaction mixture, and stirring was continued for an additional 1 h. The solvent was evaporated under vacuum, and the residue was redissolved in MeOH and triturated with DCM to precipitate the final product. After filtration, compound **9** was isolated as white solid (45% overall yield for the three steps). ^{1}H NMR (500 MHz, D_2O, 5% ND_4OD) δ 8.50 (s, 1H), 7.63 (s, 1H), 7.30 (d, J = 8.6 Hz, 2H), 6.89 (d, J = 8.6 Hz, 2H), 3.07−3.12 (m, 1H), 2.15 (s, 3H), 1.60−1.80 (m, 2H). ^{13}C NMR (125 MHz, D_2O, 5% ND_4OD) δ 166.46, 165.63, 150.84, 144.05, 139.43, 130.99, 129.17, 128.89, 125.61, 114.32, 30.81, 28.93 (d, J = 129.6 Hz), 20.36. ^{31}P NMR (162 MHz, D_2O, 5% ND_4OD) δ 19.53. HRMS (ESI−) m/z 333.0541 calculated for $C_{15}H_{14}N_2O_3PS$; found m/z 333.0473 $[M - H]^-$.

*2-((6-(p-Tolyl)thieno[2,3-d]pyrimidin-4-yl)amino)acetic Acid (**10**).* The compound was isolated as a white solid (13.8 mg, 60% yield). ^{1}H NMR (500 MHz, DMSO-d_6) δ 8.34 (s, 1H), 7.99 (s, 1H), 7.58 (d, J = 8.1 Hz, 2H), 7.32 (d, J = 8.1 Hz, 2H), 5.76 (s, 1H), 4.18 (d, J = 4.7 Hz, 2H), 2.35 (s, 3H). ^{13}C NMR (75 MHz, DMSO-d_6) δ 171.5, 164.8, 156.5, 153.6, 138.8, 138.3, 130.4, 130.0, 125.6, 117.7, 114.4, 55.0, 20.8. HRMS (ESI−) m/z 298.0656 calculated for $C_{15}H_{12}N_3O_2S$; found m/z 298.0654 $[M - H]^-$.

*(((6-(3-Chloro-4-methylphenyl)thieno[2,3-d]pyrimidin-4-yl)-amino)methyl)phosphonic Acid (**11**).* Compound **11** was isolated as a pale-yellow powder (8.5 mg, 25% overall isolated yield for the last two steps). ^{1}H NMR (400 MHz, D_2O, 5% ND_4OD) δ 8.05 (s, 1H), 7.42 (s, 1H), 7.28 (s, 1H), 7.23 (d, J = 8.0 Hz, 1H), 7.05 (d, J = 8.0 Hz, 1H), 3.44 (d, J = 13.2 Hz, 2H), 2.19 (s, 3H). ^{13}C NMR (126 MHz, D_2O, 5% ND_4OD) δ 162.6, 156.4, 152.5, 138.2, 136.0, 134.0, 131.5, 131.0, 125.0, 123.5, 118.0, 114.2, 40.3 (d, J = 134 Hz), 19.0. ^{31}P NMR (202 MHz, D_2O, 5% ND_4OD): δ 13.67. HRMS (ESI−) m/z 368.0031 calculated for $C_{14}H_{12}ClN_3O_3PS$; found m/z 368.0030 $[M - H]^-$.

*(((6-(3-Chloro-4-methylphenyl)thieno[2,3-d]pyrimidin-4-yl)-amino)(phenyl)methyl)phosphonic Acid (**12**).* Compound **12** was isolated as a white solid (20.8 mg, 48% yield for the last two steps). ^{1}H NMR (500 MHz, D_2O, 5% ND_4OD) δ 7.77 (s, 1H), 7.49 (d, J = 7.7 Hz, 3H), 7.35 (t, J = 7.2 Hz, 2H), 7.25, −7.22 (m, 1H), 7.05 (s, 1H), 6.79 (s, 1H), 6.27 (d, J = 7.2 Hz, 1H), 5.00 (d, J = 19.7 Hz, 1H), 1.75 (s, 3H). ^{13}C NMR (126 MHz, D_2O, 5% ND_4OD) δ 162.8, 155.8, 152.2, 140.9, 138.4, 135.6, 131.2, 128.1, 127.8, 126.6, 124.8, 123.2, 118.1, 114.0, 110.0, 55.5 (d, J = 134 Hz), 18.6. ^{31}P NMR (81 MHz, D_2O, 5% ND_4OD) δ 13.84. HRMS (ESI−) m/z 444.0344 calculated for $C_{20}H_{16}ClN_3O_3PS$; found m/z 444.0352 $[M - H]^-$.

*6-Bromo-4-chlorothieno[2,3-d]pyrimidine (**14**).* Thieno[2,3-d]-pyrimidin-4(3H)-one (**13**) was prepared from 2,5-dihydroxy-1,4-dithiane as previously reported,[16] with the exception that all reactions were carried out under thermal conditions. Conversion of intermediate **13** to **14** was achieved by successive reaction of **13** with Br_2 and $POCl_3$ as previously reported.[30] The 6-bromothieno[2,3-d]pyrimidin-4(3H)-one intermediate was obtained as a light-brown solid in 63% yield. The ^{1}H NMR data was consistent with the literature: ^{1}H NMR (300 MHz, DMSO-d_6) δ 12.64 (bs, 1H), 8.15 (s, 1H), 7.56 (s, 1H)]. The 6-bromo-4-chlorothieno[2,3-d]pyrimidine (**14**) was obtained as a yellow solid in 58% yield. The ^{1}H NMR data was also consistent with the literature: ^{1}H NMR (500 MHz, $CDCl_3$) δ 8.81 (s, 1H), 7.48 (s, 1H)].

*6-(p-Tolyl)thieno[2,3-d]pyrimidine-4-carbaldehyde (**15**). Step f (Scheme 1).* The common building block 4-chloro-6-(*p*-tolyl)thieno-[2,3-d]pyrimidine (50 mg, 0.19 mmol, 1 equiv) was mixed with potassium vinyltrifluoroborate (28 mg, 0.21 mmol, 1.1 equiv) and $PdCl_2(dppf)CH_2Cl_2$ (8 mg, 0.01 mmol, 0.05 equiv) and purged with argon. *i*-PrOH/H_2O (2 mL, 2/1 ratio) and Et_3N (58 mg, 0.58 mmol, 3 equiv) were added, and the mixture was purged again with argon. The mixture was sealed in pressure vessel and was heated at 100 °C for 1 h. The reaction mixture was cooled to RT, then filtered through Celite, washed with EtOAc, concentrated, and purified by chromatography (100% Hex to 20% EtOAc in Hex) on silica gel to give the C-4 vinyl intermediate 6-(*p*-tolyl)-4-vinylthieno[2,3-d]pyrimidine as yellow solid (35 mg; 72% yield). The ^{1}H NMR and MS were consistent with the desired product. ^{1}H NMR ($CDCl_3$): δ 2.40 (s, 3H, $-CH_3$), 5.85 (d, J = 10.70 Hz, 1 H), 6.77 (d, J = 10.70 Hz), 7.16−7.23 (m, 1H), 7.26 (d, J = 8.10 Hz, 2H), 7.57 (s, 1H), 7.60 (d, J = 8.10 Hz, 2H), 8.97 (s, 1H). MS (ESI+) m/z 255.1 $[M + H]^+$ for $C_{15}H_{14}N_2S$.

Step g (Scheme 1). To a solution of the above 4-vinyl-thienopyrimidine (50 mg, 0.2 mmol) in acetone:H_2O (4 mL; 10:1 ratio), 2,6-lutidine (42 mg, 0.4 mmol, 2 equiv), 4-methylmorpholine-*N*-oxide (35 mg, 0.3 mmol, 1.5 equiv), and osmium tetroxide (0.1 mL of a 40.4 mM solution in toluene) were added. The mixture was stirred for 2 h at RT (at which point LCMS indicated complete conversion to the desirable diol). Then, 1 mL of H_2O was added followed by $NaIO_4$ in small portions, and the mixture was stirred at RT for 1 h. The reaction was quenched with saturated aqueous solution of sodium thiosulfate (10 mL), and the mixture was extracted with ethyl acetate (3 × 15 mL), washed with saturated aqueous solution of ammonium chloride, dried over anhydrous $MgSO_4$, and concentrated under vacuum. The crude residue was purified by flash column chromatography on silica gel eluted with hexane−ethyl acetate (7:1) to give the aldehyde **15** as a yellow solid (32 mg, 64% yield). ^{1}H NMR ($CDCl_3$) δ: 2.43 (s, 3H), 7.30 (d, J = 8.00 Hz, 2H), 7.70 (d, J = 8.10 Hz, 2H), 8.31 (s, 1H), 9.24 (s, 1H), 10.25 (s, 1H). ^{13}C NMR (125 MHz, $CDCl_3$) δ 194.20, 171.65, 152.77, 150.54, 149.08, 140.65, 129.98, 129.81, 128.84, 127.01, 114.19, 21.40. MS (ESI+) m/z 255.12 $[M + H]^+$ for $C_{14}H_{11}N_2OS$.

*Diethyl (Amino(phenyl)methyl)phosphonate (**16b**).* In a round-bottom flask, benzaldehyde (742.79 mg, 7.00 mmol, 1 equiv) was mixed with magnesium perchlorate (156.23 mg, 0.7 mmol, 0.1 equiv) for 15 min. Benzylamine (750 mg, 7.00 mmol, 1 equiv) and diethylphosphite (0.939 mL, 7.28 mmol, 1.04 equiv) were added, and the reaction mixture was heated at 85 °C for 24 h. The crude product was dried under vacuum and purified by column chromatography on silica gel to give the diethyl ((benzylamino)-(phenyl)methyl) phosphonate product as a slightly yellow oil in 81% yield (1.8 g). ^{1}H NMR (300 MHz, $CDCl_3$) 7.43−7.28 (m, 10H), 4.15−3.80 (m, 7H), δ 3.56 (d, J = 13.3 Hz, 1H), 2.12 (s, 1H), 1.29 (t, J = 7.0 Hz, 3H), 1.14 (t, J = 7.0 Hz, 3H).[31] Hydrogenation of the diethyl ((benzylamino)(phenyl)methyl)phosphonate intermediate (200 mg, 0.6 mmol) in 4.4% formic acid in methanol (6 mL) using Pearlman's catalyst (84.25 mg, 0.6 mmol, 0.2 equiv) under argon for 2 h gave the desired crude product,[32] which was purified by column chromatography on silica gel to give the free amine as a transparent oil (145.9 mg, quantitative yield). ^{1}H NMR (500 MHz, $CDCl_3$) δ 7.45 (d, J = 7.7

dx.doi.org/10.1021/jm500629e | J. Med. Chem. 2014, 57, 5764−5776

Hz, 2H), 7.35 (t, J = 7.7 Hz, 2H), 7.30 (dd, J = 7.3, 2.0 Hz, 1H), 4.26 (d, J = 17.1 Hz, 1H),4.08−402 (m, 2H), 4.02−3.94 (m, 1H), 3.90−3.84 (m, 1H), 1.92 (br s, 2H), 1.27 (t, J = 7.0 Hz, 3H), 1.18 (t, J = 7.0 Hz, 3H).

*Diethyl (((6-Bromothieno[2,3-d]pyrimidin-4-yl)amino)methyl)-phosphonate (**17a**; R_2 = H).* The product was isolated as yellow solid (884 mg, 50% yield). ^{1}H NMR (400 MHz, CD_3OD): δ 8.36 (s, 1H), 7.56 (s, 1H), 4.20−4.12 (m, 6H), 1.28 (t, J = 7.1 Hz, 6H). ^{13}C NMR (75 MHz, CD_3OD): δ 167.7, 157.0 (d, J = 1.7 Hz), 154.8, 122.8, 118.8, 112.7, 64.1 (d, J = 6.7 Hz), 36.7 (d, J = 158 Hz), 16.7 (d, J = 5.9 Hz). ^{31}P NMR (81 MHz, CD_3OD): δ 23.91. MS (ESI+) m/z 380.10 $[M + H]^+$ for $C_{11}H_{15}BrN_3O_3PS$.

*Diethyl (((6-Bromothieno[2,3-d]pyrimidin-4-yl)amino)(phenyl)-methyl)phosphonate (**17b**; R_2 = Ph).* The product was isolated as a white solid (51 mg, 36% yield). ^{1}H NMR (300 MHz, $CDCl_3$) δ 8.42 (s, 1H), 8.11−8.07 (m, 1H), 7.70−7.67 (m, 3H), 7.27−7.22 (m, 2H), 6.32 (dd, J = 22.4, 9.6 Hz, 1H), 4.31−4.07 (m, 3H), 3.93−3.84 (m, 1H), 1.28−1.19 (s, 6H). ^{13}C NMR (75 MHz, $CDCl_3$) δ 167.7, 155.0 (d, J = 9 Hz), 153.7, 128.49 (d, J = 2 Hz), 128.44 (d, J = 2 Hz), 127.99 (d, J = 3 Hz), 121.7, 117.8, 111.3, 63.5 (d, J = 7 Hz), 50.79 (d, J = 156 Hz), 16.3 (dd, J = 19, 6 Hz). MS (ESI+) m/z 456.14 $[M + H]^+$ for $C_{17}H_{21}BrN_3O_3PS$

*Diethyl (((6-(p-Tolyl)thieno[2,3-d]pyrimidin-4-yl)amino)methyl)-phosphonate (**18a**; R_2 = R_3 = H).* The product was isolated as a white solid (25.5 mg, 65% yields). ^{1}H NMR (500 MHz, CD_3OD): δ 8.35 (s, 1H), 7.68 (s, 1H), 7.56 (d, J = 8.1 Hz, 2H), 7.25 (d, J = 8.1 Hz, 2H), 4.20−4.14 (m, 6H), 2.36 (s, 3H), 1.29 (t, J = 7.1 Hz, 6H). ^{13}C NMR (126 MHz, CD_3OD): δ 164.4, 156.4, 152.8, 140.8, 138.8, 130.5, 129.4, 125.6, 118.2, 112.7, 62.7 (d, J = 6.7 Hz), 35.3 (d, J = 158.1 Hz), 19.8, 15.3 (d, J = 5.9 Hz). _^{31}P NMR (81 MHz, CD_3OD): δ 25.16. MS (ESI+) m/z 391.9 $[M + H]^+$ for $C_{18}H_{23}N_3O_3PS$.

*Diethyl (((6-(3-Chloro-4-methylphenyl)thieno[2,3-d]pyrimidin-4-yl)amino)methyl)phosphonate (**18b**; R_2 = H, R_3 = Cl).* The product was isolated as a pale-orange solid (9.6 mg, 29% yield). ^{1}H NMR (500 MHz, CD_3OD) δ 8.38 (s, 1H), 7.76 (s, 1H), 7.39 (t, J = 9.4 Hz, 2H), 7.32 (t, J = 7.9 Hz, 1H), 4.21−4.14 (m, 6H), 2.30 (s, 3H), 1.29 (t, J = 7.1 Hz, 6H). ^{31}P NMR (202 MHz, CD_3OD) δ 23.67. MS (ESI+) m/z 426.3 $[M + H]^+$ for $C_{18}H_{22}ClN_3O_3PS$.

*Diethyl (((6-(3-Chloro-4-methylphenyl)thieno[2,3-d]pyrimidin-4-yl)amino)(phenyl)methyl)phosphonate (**18c**; R_2 = Ph, R_3 = Cl).* The product was isolated as a pale-yellow solid (27.2 mg, 60% yield). ^{1}H NMR (400 MHz, $CDCl_3$) δ 8.46 (s, 1H), 7.74 (s, 1H), 7.72 (s, 2H), 7.53 (d, J = 1.6 Hz, 1H), 7.31−7.20 (m, 5H), 6.32 (d, J = 22.0 Hz, 1H), 4.31−4.14 (m, 2H), 4.02−3.93 (m, 1H), 3.78−3.68 (m, 1H), 2.39 (s, 3H), 1.23 (t, J = 7.0 Hz, 3H), 1.06 (t, J = 7.0 Hz, 3H). ^{13}C NMR (75 MHz, $CDCl_3$) δ 166.4, 155.9 (d, J = 9 Hz), 153.6, 138.9, 136.3, 135.5, 134.9, 133.0, 131.3, 128.6, 128.6, 128.1 (d, J = 3 Hz), 126.6, 124.6, 118.3, 114.3, 63.5 (d, J = 7 Hz), 51.8 (d, J = 155 Hz), 49.8, 19.9, 16.4 (d, J = 6 Hz), 16.0 (d, J = 6 Hz). ^{31}P NMR (81 MHz, $CDCl_3$) δ 21.64. MS (ESI+) m/z 502.25 $[M + H]^+$ for $C_{24}H_{26}ClN_3O_3PS$.

In Vitro Inhibition Assays. In vitro enzymatic assays were carried out using method 2 (M2) as previously described.[12d]

Differential Scanning Fluorimetry Studies. DSF studies were carried out using the general conditions previously described.[1c] Samples were prepared to a final volume of 25 μL containing 4 μM hFPPS protein, 10 mM HEPES (pH 7.5), 10 mM NaCl, with or without 5 mM $MgCl_2$, and 5× SYPRO Orange dye (diluted from commercial stock solution of 5000×; Invitrogen). All samples were prepared in triplicate. Fluorescence was measured using an iCycler RT-PCR instrument with an iQ5 detector (Bio-Rad) while increasing the temperature gradient from 30 to 90 °C in increments of 0.5 °C/10 s. The midpoint temperature of the unfolding protein transition (T_m) was calculated using the software package from Bio-Rad iQ5. The inhibitor and substrate concentrations for each experiment are indicated in the figures.

Isothermal Titration Calorimetry (ITC) Studies. ITC experiments were carried out at 30 °C with a MicroCal iTC$_{200}$ system from GE Healthcare. The protein and ligand solutions were prepared in the same buffer (10 mM HEPES (pH 7.5), 500 mM $NaCl_2$, 2 mM β-mercaptoethanol, and 5% glycerol) at 50 μM and 1 mM concentrations, respectively. Each experiment consisted of a first 1 μL injection of the ligand followed by 18 2 μL injections into the cell containing 200 μL of the protein sample. Heats of dilution were measured in control titrations and subtracted from the actual data. The data were analyzed with the Origin 7 software provided with the instrument.

Evaluation of Competitive Binding by ^{1}H Line Broadening NMR. Spectra were acquired on a 500 MHz Varian INOVA instrument, with a HCN cold probe and z-axis pulsed-field gradients, at the Quebec/Eastern Canada High Field NMR Facility. ^{1}H NMR spectra were acquired with a 1D presaturation sequence, with a sweep width of 8000 Hz and an acquisition time of 1 s. A low power saturation pulse was applied at the HOD frequency during the 3 s relaxation delay. A 5 mm NMR tube was charged with 540 μL of D_2O and 6 μL of an inhibitor (10 mM stock solution in H_2O), and the tube was briefly mixed using a vortex. The ^{1}H NMR spectrum was acquired and the water-suppression parameters were determined (presaturation). Buffer solution (60 μL) was added to the NMR tube and briefly mixed for a final inhibitor concentration of 100 μM in buffer containing 50 mM Tris buffer at pH 7.7, 2 mM $MgCl_2$, 0.5 mM TCEP, and 20 μg/mL BSA. The ^{1}H NMR spectrum was acquired of the free inhibitor. Aliquots of the hFPPS solution in buffer (containing 22.63 μg/μL protein, 50 mM Tris at pH 7.7, 500 mM NaCl, 5% glycerol, and 0.5 mM TCEP) were added, followed by *gentle* mixing, to bring the inhibitor to hFPPS ratio as indicated on each Figure. Finally, a second inhibitor or IPP (purchased from Isoprenoids, LC, as its ammonium salt; 40 mM solution was prepared in 0.5 mM Tris buffer at pH 7.7) was added in incremental amounts to obtain the indicated ratios and confirm whether binding of the two inhibitors was competitive or not (usually titration with the second inhibitor was continued until the resonances of the first inhibitor were restored, or up to the molar ratio of hFPPS: inhibitor A; inhibitor B indicated on the NMR spectra).

Co-crystallization of hFPPS with Inhibitors 6a and 7 in the Absence of Magnesium Ions. Compounds **6a** and 7 were prepared as 100 and 25 mM stock solutions in 100 mM TrisHCl (pH 7.5) buffer, respectively. Each stock solution was added to the purified hFPPS sample to give the final concentrations of 5 mM inhibitor and 0.25 mM protein. A microseeding technique was employed to obtain crystals suitable for X-ray diffraction analysis. Crystals were grown at 22 °C by vapor diffusion in sitting drops composed of 1 μL of protein/inhibitor mixture and 1 μL of crystallization buffer, and an additional 0.5 μL of seed solution when added. Seed solutions were prepared with Seed Bead kits (Hampton Research). For the hFPPS/**6a**$^{(allo)}$ complex, the initial crystals formed in a crystallization solution composed of 0.1 M TrisHCl (pH 8.5) and 2 M ammonium dihydrogen phosphate. Diffraction quality crystals were obtained in a seeding optimization trial with a new crystallization buffer composed of 0.085 M HEPES (pH 7.5), 17% (w/v) PEG 10K, 6.8% (v/v) ethylene glycol, and 15% (v/v) glycerol. For the hFPPS/**7** complex, a single crystal was obtained under the same condition, but with microseeds prepared from the hFPPS/**6a** crystals.

X-ray Data Collection, Processing, and Structure Refinement. For structure determination, diffraction data were collected from single crystals at 100 K with synchrotron radiation (Canadian Light Source, Saskatoon, SK) and a Rayonix MX300 CCD detector. The data were processed with the *xia2* package.[33] The initial structure models were built by difference Fourier methods with a ligand/solvent-omitted input model generated from the PDB entry 2F7M. The models were improved through iterative rounds of manual and automated refinement with COOT[34] and REFMAC5.[35] The final models were deposited into the Protein Data Bank. To measure the anomalous signal from the phosphorus and sulfur atoms in the hFPPS/**6a**$^{(allo)}$ complex, additional data were collected from a single crystal at 100 K with a MicroMax-007 HF generator (Rigaku) and a Saturn 944+ CCD detector (Rigaku). This data set was also processed with the *xia2* package but without merging the Friedel mates. An anomalous density map was calculated from the processed data with the programs SHELXC[36] and ANODE.[37] Data collection and

dx.doi.org/10.1021/jm500629e | J. Med. Chem. 2014, 57, 5764−5776

Table 3. Data Collection and Refinement Statistics

	data set 1 (synchrotron) inhibitor **6a**, Pi	data set 2 (home source) inhibitor **6a**, Pi	data set 3 (synchrotron) inhibitor **7**, Pi
PDB ID	4LPG		4LPH
	Data Collection		
wavelength (Å)	0.979 49	1.5418	0.979 49
space group	$P4_12_12$	$P4_12_12$	$P4_12_12$
unit cell (Å)	$a = b = 110.87$, $c = 77.03$	$a = b = 110.96$, $c = 76.97$	$a = b = 111.12$, $c = 77.19$
resolution (Å)[a]	49.58−2.35 (2.41−2.35)	39.23−2.61 (2.67−2.61)	55.06−2.30 (2.36−2.30)
redundancy	14.4 (14.4)	7.2 (4.7)	9.4 (9.5)
completeness (%)	99.7 (98.0)	98.7 (99.0)	98.4 (99.1)
$I/\sigma(I)$	36.7 (5.4)	39.3 (5.5)	22.3 (4.8)
R_{merge}	0.044 (0.527)		0.055 (0.411)
	Refinement		
no. reflections	19406		20290
no. protein atoms	2666		2700
no. ligand atoms	31		27
no. solvent atoms	40		50
R_{work}/R_{free}	0.182/0.230		0.183/0.226
average B factor (Å^2)			
protein atoms	73.9		78.9
ligand atoms	80.4		93.4
rms deviations			
bond length (Å)	0.016		0.017
bond angle (deg)	1.8		1.8

[a]Values in parentheses are for the highest resolution shell.

refinement statistics, as well as the PDB IDs for the structure models, are presented in Table 3.

Studies on Genetic Associations. Using a cohort of 751 pairs of Alzheimer and age-matched control French Canadian subjects from a population isolate from eastern Canada, we performed the mapping of some 535000 polymorphisms in each of our case and control subjects using the Illumina 550k Human Quad genomic beadchip according to methodology reported previously.[38] Five single nucleotide polymorphisms (SNPs) were examined in the human FPPS gene loci. A specific genetic associations between variant rs4971072 (A/G) in the promoter area of hFPPS and Tau protein levels ($p < 0.02$) in the cortical area was found to be significantly associated with phospho-tau concentrations ($p < 0.02$) in the same brain region in the AD cohort.

Analysis of mRNA Prevalence. A subset of AD ($n = 34$) and age-matched control brains ($n = 24$) were used to quantify the mRNA prevalence of hFPPS using real time quantitative polymerase chain reaction (QrtPCR) as adapted from our previous studies.[28]

Total Tau Protein and Phospho-Tau Levels in the Alzheimer's Brain and in Response to hFPPS Inhibitors. Frontal cortex brain samples from autopsy-confirmed cases of Alzheimer's disease and age-matched control subjects were obtained from the Douglas Institute Brain Bank, Montreal, Canada. Frozen brain samples ($n = 116$) were homogenized and prepared according to a previously established protocol[27] prior to ELISA quantification for total cortical tau protein and phospho-tau levels. Human neuroblastoma cell cultures (SH-Sy5y from the ATCC collection) were used to assay the effects of our newly developed hFPPS inhibitors on tau metabolism and general toxicity. Typically, cells were grown in serum condition for 5 days and then exposed to different concentrations (1−500 nM) of our inhibitors for a period of 24 h. Cell were washed and lysed prior to tau and phospho-tau ELISA quantification. Total tau (T-Tau) and phospho-tau (P-Tau) concentrations were measured using a commercial enzyme immunoassay (Innotest Inc., Ghent, Belgium). In this assay, the wells of polystyrene microtiter plates were coated with the solid phase anti-human tau monoclonal antibody (AT120 for tau and AT270 for phospho-tau). The test samples were incubated in these wells along with two separate biotinylated tau monoclonal antibodies (H57 and BT2) that recognize different tau and P-Tau epitopes. Samples were rinsed with an assay buffer and then incubated with peroxidase-labeled streptavidin. Samples were subsequently incubated with tetramethylbenzidine and 0.006% hydrogen peroxide per manufacturer's instructions. The reaction was stopped with diluted sulfuric acid and optical density measurements read using a Molecular Devices Spectramax Plus plate reader. Intra-assay and interassay variability measures were 5.1% and 9.1%, consistent with manufacturer recommendation.

Lactate Dehydrogenase Assay (LDH). Lactate dehydrogenase activity was measured using a commercial kit. Maximum toxicity was based on % lactic acid dehydrogenase activity observed in the medium of cells treated with an hFPPS inhibitor as compared to the control (untreated cells); activity observed in the untreated control cells was set to 0%.

■ ASSOCIATED CONTENT

Ⓢ Supporting Information

NMR spectra and homogeneity data for inhibitors **7**−**12**. ^{1}H NMR competition studies and X-ray data. Genetic analysis on hFPPS polymorphisms. This material is available free of charge via the Internet at http://pubs.acs.org.

Accession Codes

The following codes have been deposited in the Protein Data Bank: 4LPG (hFPPS/**6a**/Pi complex) and 4LPH (hFPPS/**7**/Pi complex).

■ AUTHOR INFORMATION

Corresponding Author

*Phone 514-398-3638. Fax 514-398-3797. E-mail: Youla.tsantrizos@mcgill.ca.

Author Contributions

[#]J. W. De Schutter and J. Park contributed equally to the work described in this manuscript.

Notes

The authors declare no competing financial interest.

[∇]Zheping Hu: Undergraduate Research Participant.

■ ACKNOWLEDGMENTS

We thank Dr. Alexios Matralis for contributing to the synthesis of some key building blocks. ^{1}H NMR experiments were acquired on a 500 MHz NMR instrument at the Québec/Eastern Canada High Field NMR Facility, supported by the Natural Sciences and Engineering Research Council of Canada (NSERC), the Canada Foundation for Innovation (CFI), the Québec Ministère de la Recherche en Science et Technologie (FQRNT), and McGill University. Financial support for this work was provided by NSERC and FQRNT (research grants to Y. S. Tsantrizos) and the Canadian Institute of Health Research (CIHR; research grants to A. M. Berghuis, J. Poirier, and Y. S. Tsantrizos).

■ ABBREVIATIONS USED

hFPPS, human farnesyl pyrophosphate synthase; hGGPPS, human geranylgeranyl pyrophosphate synthase; hSQS, human squalene synthase; DMAPP, dimethylallyl pyrophosphate; IPP, isopentenyl pyrophosphate; GPP, geranyl pyrophosphate; *N*-BPs, nitrogen-containing bisphosphonates; GTPases, small guanine triphosphate binding proteins; IFNγ, interferon-gamma; SAR, structure−activity relationship; DSF, differential scanning fluorimetry; AD, Alzheimer's disease; P-Tau, phosphorylated tau; phospho-tau, phosphorylated tau; T-Tau, total tau protein; LDH, lactate dehydrogenase

■ REFERENCES

(1) (a) Rondeau, J.-M.; Bitsch, F.; Bourgier, E.; Geiser, M.; Hemmig, R.; Kroemer, M.; Lehmann, S.; Ramage, P.; Rieffel, S.; Strauss, A.; Green, J. R.; Jahnke, W. Structural basis for the exceptional in vivo efficacy of bisphosphonate drugs. *ChemMedChem* **2006**, *1*, 267−273. (b) Kavanagh, K. L.; Guo, K.; Dunford, J. E.; Wu, X.; Knapp, S.; Ebetino, F. H.; Rogers, M. J.; Russell, R. G. G.; Oppermann, U. The molecular mechanism of nitrogen-containing bisphosphonates as antiosteoporosis drugs. *Proc. Natl. Acad. Sci. U. S. A.* **2006**, *103*, 7829−7834. (c) Park, J.; Lin, Y.-S.; Tsantrizos, Y. S.; Berghuis, A. M. Ternary complex structures of human farnesyl pyrophosphate synthase bound with a novel inhibitor and secondary ligands provide insights into the molecular details of the enzyme's active site closure. *BMC Struct. Biol.* **2012**, *12*, 32.

(2) (a) Skerjanec, A.; Berenson, J.; Hsu, C.; Major, P.; Miller, W. H., Jr.; Ravera, C.; Schran, H.; Seaman, J.; Waldmeier, F. The pharmacokinetics and pharmacodynamics of zoledronic acid in cancer patients with varying degrees of renal function. *J. Clin. Pharmacol.* **2003**, *43*, 154−162. (b) Weiss, H. M.; Pfaar, U.; Schweitzer, A.; Wiegand, H.; Skerjanec, A.; Schran, H. Biodistribution and plasma protein binding of zoledronic acid. *Drug Metab. Dispos.* **2008**, *36*, 2043−2049.

(3) Morgan, G. J.; Davies, F. E.; Gregory, W. M.; Cocks, K.; Bell, S. E.; Szubert, A. J.; Navarro-Coy, N.; Drayson, M. T.; Owen, R. G.; Feyler, S.; Ashcroft, A. J.; Ross, F.; Byrne, J.; Roddie, H.; Rudin, C.; Cook, G.; Jackson, G. H.; Child, J. A. First-line treatment with zoledronic acid as compared with clodronic acid in multiple myeloma (MRC Myeloma IX): a randomized controlled trial. *Lancet* **2010**, *376*, 1989−1999.

(4) Nguyen, U. T. T.; Guo, Z.; Delon, C.; Wu, Y.; Deraeve, C.; Fränzel, B.; Bon, R. S.; Blankenfeldt, W.; Goody, R. S.; Waldmann, H.; Wolters, D.; Alexandrov, K. Analysis of the eukaryotic prenylome by isoprenoid affinity tagging. *Nature Chem. Biol.* **2009**, *5*, 227−235.

(5) Hottman, D. A.; Li, L. Protein prenylation and synaptic plasticity: implications for Alzheimer's diseases. *Mol. Neurobiol.* **2014**, DOI 10.1007/s12035-013-8627-z.

(6) (a) Morgan, G. J.; Davies, F. E.; Gregory, W. M.; Szubert, A. J.; Bell, S. E.; Drayson, M. T.; Owen, R. G.; Ashcroft, A. J.; Jackson, G. H.; Child, J. A. Effects of induction and maintenance plus long-term bisphosphonates on bone disease in patients with multiple myeloma: the Medical Research Council Myeloma IX Trial. *Blood* **2012**, *119*, 5374−5383. (b) Gnant, M.; Mlineritsch, B.; Schippinger, W.; Luschin-Ebengreuth, G.; Pöstlberger, S.; Menzel, C.; Jakesz, R.; Seifert, M.; Hubalek, M.; Bjelic-Radisic, V.; Samonigg, H.; Tausch, C.; Eidtmann, H.; Steger, G.; Kwasny, W.; Dubsky, P.; Fridrik, M.; Fitzal, F.; Stierer, M.; Rücklinger, E.; Greil, R. Endocrine therapy plus zoledronic acid in premenopaisal breast cancer. *New Engl. J. Med.* **2009**, *360*, 679−691. (c) Coleman, R. E.; Marshall, H.; Cameron, D.; Dodwell, D.; Burkinshaw, R.; Keane, M.; Gil, M.; Houston, S. J.; Grieve, R. J.; Barrett-Lee, P. J.; Ritchie, D.; Pugh, J.; Gaunt, C.; Rea, U.; Peterson, J.; Davies, C.; Hiley, V.; Gregory, W.; Bell, R. Breast-cancer adjuvant therapy with zoledronic Acid. *New Engl. J. Med.* **2011**, *365*, 1396−1405.

(7) Morita, C. T.; Jin, C.; Sarikonda, G.; Wang, H. Nonpeptide antigens, presentation mechanisms, and immunological memory of human Vγ2Vδ2 T cells: discriminating friends from foe through the recognition of prenyl pyrophosphate antigens. *Immunol. Rev.* **2007**, *215*, 59−76.

(8) (a) Eckert, G. P.; Hooff, G. P.; Strandjord, D. M.; Igbavboa, U.; Volmer, D. A.; Müller, W. E.; Wood, W. G. Regulation of the brain isoprenoids farnesyl- and geranylgeranylpyrophosphate is altered in male Alzheimer patients. *Neurobiol. Dis.* **2009**, *35*, 251−257. (b) Hooff, G. P.; Wood, W. G.; Müller, W. E.; Eckert, G. P. Isoprenoids, small GTPases and Alzheimer's diseases. *Biochim. Biophys. Acta* **2010**, *1801*, 896−905.

(9) Jahnke, W.; Rondeau, J.-M.; Cotesta, S.; Marzinzik, A.; Pellé, X.; Geiser, M.; Strauss, A.; Götte, M.; Bitsch, F.; Hemmig, R.; Henry, C.; Lehmann, S.; Glickman, J. F.; Roddy, T. P.; Stout, S. J.; Green, J. R. Allosteric non-bisphosphonate FPPS inhibitors identified by fragment-based discovery. *Nature Chem. Biol.* **2010**, *6*, 660−666.

(10) Lindert, S.; Zhu, W.; Liu, Y.-L.; Pang, R.; Oldfield, E.; McCammon, J. A. Farnesyl diphosphate synthase inhibitors from in silico screening. *Chem. Biol. Drug Des.* **2013**, *81*, 742−748.

(11) Gabelli, S. B.; McLellan, J. S.; Montalvetti, A.; Oldfield, E.; Docampo, R.; Amzel, L. M. Structure and mechanism of the farnesyl diphosphate synthase from *Trypanosoma cruzi*: implications for drug design. *Protein* **2006**, *62*, 80−88.

(12) (a) Lin, Y.-S.; Park, J.; De Schutter, J. W.; Huang, X. F.; Berghuis, A. M.; Sebag, M.; Tsantrizos, Y. S. Design and synthesis of active site inhibitors of the human farnesyl pyrophosphate synthase—apoptosis and inhibition of ERK phosphorylation in multiple myeloma cells. *J. Med. Chem.* **2012**, *55*, 3201. (b) De Schutter, J. W.; Shaw, J.; Lin, Y.-S.; Tsantrizos, Y. S. Design of potent bisphosphonate inhibitors of the human farnesyl pyrophosphate synthase via targeted interactions with the active site "capping" phenyls. *Bioorg. Med. Chem.* **2012**, *20*, 5583−5591. (c) Leung, C.-Y.; Langille, A. M.; Mancuso, J.; Tsantrizos, Y. S. Discovery of thienopyrimidine-based inhibitors of the human farnesyl pyrophosphate synthase—parallel synthesis of analogs via a trimethylsilyl ylidene intermediate. *Bioorg. Med. Chem. Lett.* **2013**, *21*, 2229−2240. (d) Leung, C. Y.; Park, J.; De Schutter, J. W.; Sebag, M.; Berghuis, A. M.; Tsantrizos, Y. S. Thienopyrimidine bisphosphonate (ThPBP) inhibitors of the human farnesyl pyrophosphate synthase: optimization and characterization of the mode of inhibition. *J. Med. Chem.* **2013**, *56*, 7939−7950.

(13) Zhang, Y.; Cao, R.; Yin, F.; Hudock, M. P.; Guo, R.-T.; Krysiak, K.; Mukherjee, S.; Gao, Y.-G.; Robinson, H.; Song, Y.; No, J. H.; Bergan, K.; Leon, A.; Cass, L.; Goddard, A.; Chang, T.-K.; Lin, F.-Y.; Van Beek, E.; Papapoulos, S.; Wang, A.H.-J.; Kubo, T.; Ochi, M.; Mukkamala, D.; Oldfield, E. Lipophilic bisphosphonates as dual farnesyl/geranylgeranyl diphosphate synthase inhibitors: an X-ray and NMR investigation. *J. Am. Chem. Soc.* **2009**, *131*, 5153−5162.

(14) Ciosek, C. P., Jr.; Magnin, D. R.; Harrity, T. W.; Logan, J. V. H.; Dickson, J. K.; Gordon, E. M.; Hamilton, K. A.; Jolibois, K. G.; Kunselman, L. K.; Lawrence, R. M.; Mookhtiar, K. A.; Rich, L. C.; Slusarchyk, D. A.; Sulsky, R. B.; Biller, S. A. Lipophilic 1,1-bisphosphonates are potent squalene synthase inhibitors and orally active cholesterol lowering agents in vivo. *J. Biol. Chem.* **1993**, *268*, 24832−24837.

(15) Dunford, J. E.; Kwaasi, A. A.; Rogers, M. J.; Barnett, B. L.; Ebetino, F. H.; Russell, R. G. G.; Oppermann, U.; Kavanagh, K. L. Structure−activity relationship among the nitrogen containing bisphosphonates in clinical use and other analogues: time-dependent inhibition of human farnesyl pyrophosphate synthase. *J. Med. Chem.* **2008**, *51*, 2187−2195.
(16) Hesse, S.; Perspicace, E.; Kirsch, G. Microwave-assisted synthesis of 2-aminothiophene-3-carboxylic acid derivatives, 3*H*-thieno[2,3-*d*]pyrimidin-4-one and 4-chlorothieno[2,3-*d*]pyrimidine. *Tetrahedron Lett.* **2007**, *48*, 5261−5264.
(17) Kálmán, F. K.; Woods, M.; Caravan, P.; Jurek, P.; Spiller, M.; Tircsó, G.; Király, R.; Brücher, E.; Sherry, A. D. Potentiometric and relaxometric properties of a gadolinium-based MRI contrast agent for sensing tissue pH. *Inorg. Chem.* **2007**, *46*, 5260−5270.
(18) Yu, W.; Mei, Y.; Kang, Y.; Hua, Z.; Jin, Z. Improved procedure for the oxidative cleavage of olefins by OsO_4-$NaIO_4$. *Org. Lett.* **2004**, *6*, 3217−3219.
(19) (a) Waszkuć, W.; Janecki, T.; Bodaiski, R. A Convenient Synthesis of α-Hydroxyaldehydes and Hydroxymethyl Ketones. *Synthesis* **1984**, 1025−1027. (b) Lahrache, H.; Robin, S.; Rousseau, G. Halodephosphorylation of α,β-unsaturated phosphonic acid monoesters. *Tetrahedron Lett.* **2005**, *46*, 1635−1637.
(20) Hoffman, A.; Ott, A.; Breteler, M. M. B.; Bots, M. L.; Slooter, A. J. C.; van Harskamp, F.; van Duijn, C. N.; Broeckhoven, C. V.; Grobbee, D. E. Atherosclerosis, apolipoprotein E, and prevalence of dementia and Alzheimer's disease in the Rotterdam Study. *Lancet* **1997**, *349*, 151−154.
(21) Marchant, N. L.; Reed, B. R.; Sanossian, N.; Madison, C. M.; Kriger, S.; Dhada, R.; Mack, W. J.; DeCarli, C. The aging brain and cognition-contribution of vascular injury and Aβ to mild cognitive dysfunction. *JAMA Neurol.* **2013**, *70*, 488−495.
(22) (a) Jick, H.; Zornberg, G. L.; Jick, S. S.; Seshadri, S.; Drachman, D. A. Statins and the risk of dementia. *Lancet* **2000**, *356*, 1627−1631. (b) Wolozin, B.; Wang, S. W.; Li, N. C.; Lee, A.; Lee, T. A.; Kazis, L. E. Simvastatin is associated with a reduced incidence of dementia and Parkinson's diseases. *BMC Med.* **2007**, *5*, 20.
(23) Riekse, R. G.; Li, G.; Petrie, E. C.; Leverenz, J. B.; Vavrek, D.; Vuletic, S.; Albers, J. J.; Montine, T. J.; Lee, V. M.; Lee, M.; Seubert, P.; Galasko, D.; Schellenberg, G. D.; Hazzard, W. R.; Peskind, E. R. Effect of statins on Alzheimer's disease biomarkers in cerebrospinal fluid. *J. Alzheimer's Dis.* **2006**, *10*, 399−406.
(24) Li, G.; Larson, E. B.; Sonnen, J. A.; Shofer, J. B.; Petrie, E. C.; Schantz, A.; Peskind, E. R.; Raskind, M. A.; Breitner, J. C. S.; Montine, T. J. Statin therapy is associated with reduced neuropathologic changes of Alzheimer disease. *Neurology* **2007**, *69*, 878−885.
(25) Hooper, C.; Killick, R.; Lovestone, S. The GSK3 hypothesis of Alzheimer's disease. *J. Neurochem.* **2008**, *104*, 1433−1439.
(26) Ballatore, C.; Lee, V.M.-Y.; Trojanowski, J. Q. Tau-mediated neurodegeneration in Alzheimer's diseases and related disorders. *Nature Rev. Neurosci.* **2007**, *8*, 663−672.
(27) Beffert, U.; Cohn, J. S.; Petit-Turcotte, C.; Tremblay, M.; Aumont, N.; Ramassamy, C.; Davignon, J.; Poirier, J. Apolipoprotein E and beta-amyloid levels in the hippocampus and frontal cortex of Alzheimer's disease subjects are disease-related and apolipoprotein E genotype dependent. *Brain Res.* **1999**, *843*, 87−94.
(28) Leduc, V.; Legault, V.; Dea, D.; Poirier, J. Normalization of gene expression using SYBR green qPCR: a case for paraoxonase 1 and 2 in Alzheimer's disease brains. *J. Neurosci. Methods* **2011**, *200*, 14−19.
(29) Mashalidis, E. H.; Śledź, P.; Lang, S.; Abell, C. A three-stage biophysical screening cascade for fragment-based drug discovery. *Nature Protoc.* **2013**, *8*, 2309−2324.
(30) Bugge, S.; Kaspersen, S. J.; Sundby, E.; Hoff, B. H. Route selection in the synthesis of C-4 and C-6 substituted thienopyrimidines. *Tetrahedron* **2012**, *68*, 9226−9233.
(31) Wu, J.; Sun, W.; Xia, H.-G.; Sun, X. A facile and highly efficient route to a-aminophosphonates via three-component reactions catalyzed by $Mg(ClO_4)_2$ or molecular iodine. *Org. Biomol. Chem.* **2006**, *4*, 1663−1666.
(32) Gray, B. D.; Jeffs, P. W. Alkylation and condensation reactions of *N,N*-dibenzylglycine esters: synthesis of a-amino acid derivatives. *J. Chem. Soc., Chem. Commun.* **1987**, 1329−1330.
(33) Winter, G. *xia2*: an expert system for macromolecular crystallography data reduction. *J. Appl. Crystallogr.* **2010**, *43*, 186−190.
(34) Emsley, P.; Cowtan, K. Coot: model-building tools for molecular graphics. *Acta Crystallogr., Sect. D: Biol. Crystallogr.* **2004**, *60*, 2126−2132.
(35) Vagin, A. A.; Steiner, R. A.; Lebedev, A. A.; Potterton, L.; McNicholas, S.; Long, F.; Murshudov, G. N. REFMAC5 dictionary: organization of prior chemical knowledge and guidelines for its use. *Acta Crystallogr., Sect. D: Biol. Crystallogr.* **2004**, *60*, 2184−2195.
(36) Sheldrick, G. M. Experimental phasing with SHELXC/D/E: combining chain tracing with density modification. *Acta Crystallogr., Sect. D: Biol. Crystallogr.* **2010**, *66*, 479−485.
(37) Thorn, A.; Sheldrick, G. M. *ANODE*: anomalous and heavy-atom density calculation. *J. Appl. Crystallogr.* **2011**, *44*, 1285−1287.
(38) Lambert, J.-C.; Heath, S.; Even, G.; Campion, D.; Sleegers, K.; Hiltunen, M.; Combarros, O.; Zelenika, D.; Bullido, M. J.; Tavernier, B.; Letenneur, L.; Bettens, K.; Berr, C.; Pasquier, F.; Fiévet, N.; Barberger-Gateau, P.; Engelborghs, S.; De Deyn, P.; Mateo, I.; Franck, A.; Helisalmi, S.; Porcellini, E.; Hanon, O.; The European Alzheimer's Disease Initiative Investigators; de Pancorbo, M. M.; Lendon, C.; Dufouil, C.; Jaillard, C.; Leveillard, T.; Alvarez, V.; Bosco, P.; Mancuso, M.; Panza, F.; Nacmias, B.; Bossù, P.; Piccardi, P.; Annoni, G.; Seripa, D.; Galimberti, D.; Hannequin, D.; Licastro, F.; Soininen, H.; Ritchie, K.; Blanché, H.; Dartigues, J.-F.; Tzourio, C.; Gut, I.; Van Broeckhoven, C.; Alpérovitch, A.; Lathrop, M.; Amouyel, P. Genome-wide association study identifies variants at *CLU* and *CR1* associated with Alzheimer's disease. *Nature Genet.* **2009**, *41*, 1094−1099.